

Thermodynamically Stable One-Component Quasicrystals: A Density-Functional Survey of Relative Stabilities

A. R. Denton* and J. Hafner

Institut für Theoretische Physik, Technische Universität Wien

Wiedner Hauptstraße 8-10, A-1040 Wien, Austria

(August 14, 2018)

Abstract

A combination of classical density-functional theory and thermodynamic perturbation theory is applied to a survey of finite-temperature trends in the relative stabilities of one-component crystals and quasicrystals interacting via effective metallic pair potentials derived from pseudopotential theory. Splitting the pair potential into a strongly repulsive short-range core and a relatively weak oscillating tail, the Helmholtz free energy functional of specified solid structures with Gaussian density distribution is computed for given thermodynamic states, and variationally minimized with respect to the width of the distribution. Comparing the free energies of several periodic crystals and rational approximant models of quasicrystals over a range of pseudopotential parameters, *thermodynamically* stable quasicrystals are predicted for parameters approaching the limits of mechanical stability of the crystal structures. Quasicrystalline stability is attributed to vibrational stiffness and energetically favorable medium- and long-range interactions. The results support and significantly extend conclusions of previous ground-state lattice-sum studies.

PACS numbers: 61.44.+p, 64.70.Dv, 61.25.Mv, 05.70.-a

Typeset using REVTeX

I. INTRODUCTION

Since the landmark discovery [1] of long-range icosahedral quasiperiodic ordering in Al-Mn alloys, thermodynamically stable quasicrystals have been produced in a rich variety of systems [2–4]. The fact remains, however, that all known quasicrystals are alloys of at least two metallic elements. A fundamental question has thus naturally arisen: can one-component quasicrystals be thermodynamically stable? An icosahedral quasiperiodic phase having lower ground-state enthalpy than periodic crystals has in fact been predicted for an idealized system of particles interacting via a square-well pair potential [5]. The stability range is confined, however, to a very narrow range of well widths and pressures and the physical relevance is unclear. On a much broader scale, the question has been addressed by extensive lattice-sum potential energy calculations [6,7] for a variety of crystals and quasicrystals interacting via effective metallic pair potentials generated by pseudopotential theory. The important conclusion of these studies is that energetically stable ground-state one-component quasicrystals are indeed possible, albeit within a restricted range of pair potential parameters having no counterparts in the Periodic Table.

Although very useful for identifying general trends in relative structural stabilities, the lattice-sum approach, because it takes into account only internal energy, is restricted to zero temperature. Therefore it cannot directly address the general issue of *thermodynamic* stability. An alternative theoretical approach, especially suited to finite temperatures, is the classical density-functional (DF) approach [8], by which the thermodynamic free energy is determined as a variational minimum with respect to density of an approximate free energy functional. Important fundamental applications have already been made to systems of hard spheres with quasiperiodic order [9,10]. Distinguished as they are by purely entropic (structure-dependent) free energy, hard-sphere (HS) systems are ideally suited for focusing exclusively on the role of entropy in stabilizing competing structures. Because the infinitely repulsive HS pair potential lacks an energy scale, however, temperature in this case is irrelevant to static properties. Comparing elementary crystals with model quasicrys-

talline structures, the quasicrystals were predicted to be either higher in free energy and thus metastable (in fact, relative even to the fluid phase) [9] or mechanically unstable (no variational minimum) [10]. These studies clearly suggest that ordinary entropy (associated with phonons and disorder) is by itself insufficient to stabilize quasiperiodic ordering. The previous lattice-sum and DF studies leave open, however, the question of whether at finite temperatures longer-range interactions can conspire to stabilize one-component quasicrystalline structures.

Our main goal in this paper is to bridge the gap between previous studies by extending classical DF methods to simple metallic systems whose effective pair interactions may be derived from pseudopotential theory. By varying the parameters that define the pair potential, we are able to systematically survey a range of physically relevant systems and thermodynamic states for the possible existence of stable one-component quasicrystals. As a structural model, we focus here on a certain class of rational approximants, periodic crystals with large unit cells whose atomic configurations realistically model quasicrystalline order. As our main result, we indeed find, over a limited range of pseudopotential parameters, thermodynamically stable one-component quasicrystals, whose stabilities are largely attributable to medium- and long-range interactions. As an incidental result, we also predict mechanically stable, but thermodynamically unstable, HS rational approximants, thus supporting conclusions of previous DF studies for HS systems [9,10].

We proceed in Sec. II by outlining the calculation of the effective metallic pair potentials. These constitute a fundamental input to the theory described in Sec. III, which combines classical DF methods with thermodynamic perturbation theory. In Sec. IV, after first describing the quasicrystal structural model, we present results, from a broad survey of pseudopotential parameters, for trends in the relative stabilities of various solid structures. Finally, in Sec. V we summarize and conclude with some remarks on the implications of our study for the stabilities of real quasicrystals.

II. INTERATOMIC INTERACTIONS IN METALS

Interactions between ions in a metal are complicated by the presence of conduction (or valence) electrons, whose response to the ions in many cases must be determined by elaborate methods of electronic DF theory [11]. However, when the energy levels of core and conduction electrons are sufficiently well separated, as they are in the simple metals (*e.g.*, Al, Mg, and the alkalis), the conduction electrons may be justly regarded as nearly free [12,13]. It then proves possible to replace the strong electron-ion potential by a much weaker *pseudopotential*, which has no bound states but preserves the true valence energy spectrum.

The pseudopotential approach [14–16] has been refined over three decades and, with remarkable success, has helped to explain a wide range of structural and thermodynamic properties of solids, including variations in crystal structure through the Periodic Table [17]. Its conceptual appeal lies in its reduction of the two-component system of electrons and ions to an effective one-component system of pseudoatoms. The reduction is achieved by regarding the pseudopotential as a weak perturbation to a uniform gas of valence electrons, which is further assumed to respond adiabatically and linearly to the effective static external potential imposed by the ions. In linear response theory, the Fourier components of the induced electron density $\hat{\rho}_e(\mathbf{k})$ and the ion density $\hat{\rho}_i(\mathbf{k})$ are simply related by

$$\hat{\rho}_e(\mathbf{k}) = \chi(k)\hat{v}^{ps}(k)\hat{\rho}_i(\mathbf{k}), \quad (1)$$

where $\chi(k)$ is the static electron-density response function. To second order in perturbation theory, the effective ion-ion pair potential then takes the Fourier-space form

$$\hat{\phi}(k) = Z^2v(k) \left[1 + \left(\frac{1}{\epsilon(k)} - 1 \right) \left(\frac{\hat{v}^{ps}(k)}{Zv(k)} \right)^2 \right], \quad (2)$$

where $v(k) = 4\pi e^2/k^2$ is the Fourier transform of the bare Coulomb interaction and $\epsilon(k)$ is the dielectric function, whose density dependence naturally gives rise to *density-dependent* effective pair potentials. The dielectric and static response functions are closely related through

$$\epsilon(k) = 1 - \left(\frac{v(k)\chi_o(k)}{1 + v(k)G(k)\chi_o(k)} \right), \quad (3)$$

where $\chi_o(k)$ is the Lindhard free electron density response function and $G(k)$ is the local field correction, which incorporates exchange and correlation effects. Experience has shown [16] that the accuracy of the effective pair potential is particularly sensitive to the choice of $G(k)$. Here we take the analytic form proposed by Ichimaru and Utsumi [18], which accurately fits Monte Carlo data for the correlation energy and satisfies important self-consistency conditions.

The choice of pseudopotential is less critical, and in practice a parametrized form is often assumed and fitted to experimental data for transport and other properties sensitive to electron-ion interactions. A particularly simple and popular form, which we have adopted here, is the (local and energy-independent) empty-core pseudopotential [19]

$$\begin{aligned} v^{ps}(r) &= 0, & r < r_c \\ &= -\frac{Ze^2}{r}, & r > r_c, \end{aligned} \quad (4)$$

parametrized by valence Z and core radius r_c . The resulting real-space effective pair potential $\phi(r)$ following from Eqs. (2-4) is illustrated in Fig. 1 for several values of atomic volume Ω (or number density $1/\Omega$), valence, and core radius as a ratio of the electron-sphere radius $r_s = (3\Omega/4\pi Z)^{1/3}$. (Note that we use atomic units throughout, representing energies in milli-Rydbergs and lengths in Bohr radii a_o .) As is typical for the simple metals, $\phi(r)$ is characterised by a steeply repulsive short-range core, arising from screening of the bare ion-ion interaction by polarization of the electrons, and a relatively weak oscillating tail, dominated by Friedel oscillations with periodicity π/k_F (k_F being the Fermi wavevector magnitude). Extensive analysis [16,17] has shown that the form of the potential in the vicinity of the nearest-neighbor distance depends sensitively on the interplay between the core and tail regions. In particular, with increasing electron density (increasing Z or decreasing Ω) at fixed r_c/r_s , the core shifts to shorter distances and the wavelength of the Friedel oscillations shortens [Fig. 1 (a) and (b)]. Correspondingly, the core repulsion steepens and the

depth of the first minimum becomes shallower as the oscillations move under the core. For sufficiently high electron density, the first minimum may be covered by the core, resulting in a repulsive shoulder, as seen in Fig. 1 (a) for the case of $Z = 3.2$. On the other hand, with decreasing core radius for fixed Z , the Friedel oscillations weaken in amplitude and shorten in wavelength. For sufficiently small r_c , the first minimum similarly may be pushed to larger distances, as seen in Fig. 1 (c) for the case $r_c/r_s = 0.4$. In Sec. IV B we discuss the influence of these properties of $\phi(r)$ on structural stabilities of solids.

III. THEORETICAL APPROACH

A. Classical Density-Functional Theory

With effective pair potentials in hand, we may now in a sense regard the electronic structure problem as solved – albeit trivially in this case – and henceforth consider, at fixed average density, a purely classical one-component system of pair-wise interacting pseudoatoms. We thus proceed to take $\phi(r)$ as input to a classical DF theory for the Helmholtz free energy, the central quantity of interest in assessing relative stabilities of competing solid structures. The DF approach [8] provides a general framework for describing nonuniform systems, of which solids are extreme examples. For classical systems, it is founded on the definition of a functional $F[\rho]$ of the spatially-varying one-particle number density $\rho(\mathbf{r})$, which satisfies a fundamental variational principle [20,21], according to which $F[\rho]$ is minimized (at constant average density) by the equilibrium density, its minimum value equaling the Helmholtz free energy. For convenience, $F[\rho]$ is separated into ideal-gas and excess contributions:

$$F[\rho] = F_{id}[\rho] + F_{ex}[\rho]. \quad (5)$$

The first term is the free energy of the nonuniform system in the absence of interactions, directly related to the configurational entropy, and is given exactly by

$$F_{id}[\rho] = k_B T \int d\mathbf{r} \rho(\mathbf{r}) [\ln(\rho(\mathbf{r})\lambda^3) - 1], \quad (6)$$

where λ is the thermal de Broglie wavelength and T is temperature. The excess contribution depends entirely upon internal interactions and is not known exactly. Approximations for $F_{ex}[\rho]$ abound, but experience has proven the class of so-called weighted-density approximations [22–24] (WDA) to be especially useful in a variety of contexts [26]. These are all based on a mapping of the nonuniform excess free energy onto its uniform counterpart, as discussed further below. It should be emphasized that here we entirely ignore a sizable volume-dependent, but structure-independent, term in the free energy associated with the electrons [12,13]. This is justified by the fact that here we are concerned only with the relative stabilities of different solid structures and thus always compare free energies of solids at the *same average density*. In applications to phase transitions, however, the volume term would have to be included for coexisting phases having different densities.

Although there have been numerous successful applications of DF theory to simple atomic systems [26] (*e.g.*, HS and Lennard-Jones potentials), few thus far have considered metals [27,28]. Studies with other long-range pair potentials have shown [29,30], however, that weighted-density methods are often best applied in combination with thermodynamic perturbation theory. The essential reason is that a single mapping proves insufficient to accurately approximate both the excess entropy and the internal energy [24,31]. As seen from Fig. 1, the basic form of $\phi(r)$ for the simple metals lends itself naturally to a perturbation approach, wherein the full pair potential is sensibly split into a short-range reference potential $\phi_o(r)$ and a perturbation potential $\phi_p(r) = \phi(r) - \phi_o(r)$. Such an approach has already been applied successfully to the structure and thermodynamics of Lennard-Jones liquids [13,32] and solids [22,24,25,33,34] and of metallic liquids [35,36] and solids [37]. The Helmholtz free energy may be correspondingly separated and formally expressed in the exact form [21]

$$F[\rho] = F_o[\rho] + \frac{1}{2} \int_0^1 d\lambda \int d\mathbf{r} \int d\mathbf{r}' \rho^{(2)}(\mathbf{r}, \mathbf{r}'; \phi_\lambda) \phi_p(|\mathbf{r} - \mathbf{r}'|), \quad (7)$$

where $\rho^{(2)}(\mathbf{r}, \mathbf{r}'; \phi_\lambda)$ is the two-particle density for a system interacting via the pair potential $\phi_\lambda(r) \equiv \phi_o(r) + \lambda\phi_p(r)$. The reference free energy $F_o[\rho]$ includes the ideal-gas free energy and the part of the excess free energy associated with short-range interactions, while the

perturbation term is the remaining part of the excess free energy deriving from medium- and long-range interactions. Further expanding $\rho^{(2)}$ about the reference pair potential, and retaining only the leading term, leads directly to the first-order perturbation approximation,

$$F[\rho] \simeq F_o[\rho] + \frac{1}{2} \int d\mathbf{r} \int d\mathbf{r}' \rho(\mathbf{r}) \rho(\mathbf{r}') g_o(\mathbf{r}, \mathbf{r}') \phi_p(|\mathbf{r} - \mathbf{r}'|), \quad (8)$$

where $g_o(\mathbf{r}, \mathbf{r}')$ is the pair distribution function of the reference system (radial distribution function for a uniform liquid). The second-order term in the perturbation expansion F_2 may be expressed in terms of the mean-square fluctuation of the total perturbation energy

$$\Phi_p \equiv \sum_{i < j} \phi_p(|\mathbf{r}_i - \mathbf{r}_j|) \quad (9)$$

according to

$$F_2 = -\frac{1}{2k_B T} \langle (\Phi_p - \langle \Phi_p \rangle_o)^2 \rangle_o, \quad (10)$$

where $\langle \dots \rangle_o$ denotes an ensemble average for the reference system. In general, the n th term in the expansion F_n may be expressed in terms of the mean fluctuations $\langle (\Phi_p - \langle \Phi_p \rangle_o)^m \rangle_o$ divided by $(k_B T)^{n-1}$, with $m \leq n$ [13,38]. Thus, roughly speaking, convergence of the expansion is determined by the magnitude of fluctuations in Φ_p relative to $k_B T$. We return to the issue of convergence in Sec. V.

Some freedom remains in the separation of the pair potential and in the choice of reference system. Here we use the standard Weeks-Chandler-Andersen [32] (WCA) separation, which splits the potential at its first minimum and shifts it such that

$$\begin{aligned} \phi_o(r) &= \phi(r) - \phi(r_{min}), & r < r_{min} \\ &= 0, & r > r_{min} \end{aligned} \quad (11)$$

and

$$\begin{aligned} \phi_p(r) &= \phi(r_{min}), & r < r_{min} \\ &= \phi(r), & r > r_{min}. \end{aligned} \quad (12)$$

The strongly repulsive reference system we map onto a system of hard spheres of effective diameter d . Although the WCA prescription [13,32] for d is usually considered superior for liquids, application to solids is problematic because the required function $g_o(\mathbf{r}, \mathbf{r}')$ is relatively poorly known (see below). Thus, we use instead the simpler Barker-Henderson prescription,

$$d = \int_0^\infty dr \{1 - \exp[-\phi_o(r)/k_B T]\}, \quad (13)$$

which for the dense liquid gives an effective diameter very close to that of the WCA prescription and in fact reduces to the latter as the steepness of $\phi_o(r)$ increases.

The reference free energy of the solid is now well approximated by the modified weighted-density approximation (MWDA), which is known to give an accurate description of HS systems [39]. This maps the excess free energy per particle of the HS solid onto that of the corresponding *uniform* fluid f_o , according to

$$F_{ex}^{MWDA}[\rho]/N = f_o(\hat{\rho}), \quad (14)$$

where the weighted density

$$\hat{\rho} \equiv \frac{1}{N} \int d\mathbf{r} \int d\mathbf{r}' \rho(\mathbf{r}) \rho(\mathbf{r}') w(|\mathbf{r} - \mathbf{r}'|; \hat{\rho}) \quad (15)$$

is a self-consistently determined weighted average of the physical density. The associated weight function w is in turn specified by the normalization condition

$$\int d\mathbf{r}' w(|\mathbf{r} - \mathbf{r}'|) = 1, \quad (16)$$

and by the requirement that $F_{ex}^{MWDA}[\rho]$ generate the exact two-particle (Ornstein-Zernike) direct correlation function $c(r)$ in the uniform limit:

$$\lim_{\rho(\mathbf{r}) \rightarrow \rho} \left(\frac{\delta^2 F_{ex}[\rho]}{\delta \rho(\mathbf{r}) \delta \rho(\mathbf{r}')} \right) = -k_B T c(|\mathbf{r} - \mathbf{r}'|; \rho). \quad (17)$$

Equations (16) and (17) lead to a simple analytic relation [39] between $w(r)$ and the fluid-state functions f_o and $c(r)$, computed here using the convenient expressions following from

the analytic solution of the Percus-Yevick integral equation for hard spheres [13], which are sufficiently accurate when evaluated at the relatively low weighted densities of relevance.

In principle, the perturbation free energy F_p [second term in Eq. (8)] demands detailed knowledge of the HS solid pair distribution function $g_{HS}(\mathbf{r}, \mathbf{r}'; d)$. Although its translational average is partially known from Monte Carlo studies [40], the published data and analytic fits are limited to particular solid structures (close-packed crystals) at specific densities. In many applications, however, the function is needed over a range of densities, and here also for a variety of solid structures. For practical purposes, various approximations for F_p have been proposed. Jones and Ashcroft [25] and Curtin [41] have calculated the free energy of the LJ solid by approximating the spherical average of the two-particle density in the solid by that in the isotropic liquid, thereby ignoring any dependence upon solid structure. Clearly this is insufficient for comparing relative stabilities of different solid structures. Curtin and Ashcroft [24] have derived a structure-dependent correction, involving the difference between the true and reference system direct correlation functions, and have employed an empirical prescription to study the Lennard-Jones crystal. More recently, Mederos *et al.* [34] have proposed, in the spirit of the WDA, mapping the pair distribution function of the solid onto the corresponding radial distribution function of the fluid, but evaluated at an effective density chosen to satisfy a local compressibility relation. In practice, the requisite density is found to be so low that the approximation is essentially equivalent to replacing $g_{HS}(\mathbf{r}, \mathbf{r}'; d)$ by its ideal-gas limit, the Heaviside unit step function $u(|\mathbf{r} - \mathbf{r}'| - d)$, defined by

$$\begin{aligned} u(x) &= 0, & x < 0 \\ &= 1, & x > 0. \end{aligned} \tag{18}$$

This amounts to a mean-field approximation in which self-correlations are forbidden but correlations are otherwise entirely neglected. The underlying justification [23] is the fact that in an ordered solid, unlike in a dense liquid, most of the structure of the two-particle density is contained already at the level of the one-particle density, rendering $g(\mathbf{r}, \mathbf{r}')$ a relatively structureless function. Because of its practicality and its success when applied to

the Lennard-Jones [34] and other [42,43] systems, we have adopted this approximation for the perturbation free energy.

Finally, collecting together the above-mentioned DF and perturbation approximations, our working free energy functional is expressed as

$$F[\rho] \simeq F_{HS}^{MWDA}[\rho; d] + \frac{1}{2} \int d\mathbf{r} \int d\mathbf{r}' \rho(\mathbf{r}) \rho(\mathbf{r}') u(|\mathbf{r} - \mathbf{r}'| - d) \phi_p(|\mathbf{r} - \mathbf{r}'|), \quad (19)$$

which is to be variationally minimized with respect to the solid number density $\rho(\mathbf{r})$. The perturbation free energy evidently amounts to a lattice-sum over $\phi_p(r)$, but one that incorporates thermal broadening of the density distribution. Note that the temperature dependence of the total free energy consists of a trivial (linear) dependence of the HS reference free energy and a non-trivial dependence through the effective HS diameter d [Eq. (13)].

The free energy of the liquid phase is calculated, at the same level of perturbation theory, via the uniform limit of Eq. (8). Here the reference system free energy is very accurately approximated by the Carnahan-Starling excess free energy of the HS fluid [13]. For the perturbation, however, a mean field approximation is inappropriate, since the radial distribution function of the dense HS fluid is far more structured than that of the solid. Therefore, instead of Eq. (18), we use the highly accurate Verlet-Weis fit to simulation data for the fluid function $g_{HS}(r)$.

B. Practical Implementation

Calculation of the free energy based on the approximate functional (19) requires, in practice, specification of the solid structure, *i.e.*, the position vectors \mathbf{R} of the equilibrium atomic sites. Here we consider three elementary crystal structures (fcc, hcp, and bcc) and, as a model of quasicrystalline structure, a sequence of rational approximants [2,44]. The fcc and bcc crystals are Bravais lattices, characterized – in fact, defined – by equivalence of every lattice site [45]. The hcp structure, is composed of two interpenetrating simple-haxagonal Bravais lattices or, equivalently, one simple-hexagonal lattice with a two-atom basis. The

rational approximants are experimentally observed periodic crystals with large unit cells, whose structures realistically model the atomic ordering of certain known quasicrystals. Their structures are described in detail in Sec. IV A. For practical purposes, here we regard them as consisting of a simple-cubic Bravais lattice together with a multi-atom basis.

In addition to the positions of the atomic sites, the density distribution about the sites must in practice be specified. A particularly simple and widely adopted ansatz for the density distribution [22,26] places normalized isotropic Gaussians at the sites of the solid, according to

$$\rho(\mathbf{r}) = \left(\frac{\alpha}{\pi}\right)^{3/2} \sum_{\mathbf{R}} \sum_{\mathbf{d}} \exp(-\alpha|\mathbf{r} - \mathbf{R} - \mathbf{d}|^2). \quad (20)$$

Here the first sum is over the sites (or unit cells) of the underlying Bravais lattice and the second is over the basis atoms, whose positions are described by displacements \mathbf{d} relative to the lattice sites. The parameter α determines the width of the distribution and represents the single variational parameter with respect to which the free energy functional is minimized. The Gaussian ansatz has been shown by simulation [46,47] and by numerical analysis [48] to yield a reasonably accurate approximation to the true density distribution in close-packed Bravais crystals near melting, despite deviations in the detailed form of the distribution, and it has been widely and successfully used in diverse applications of classical DF theory to thermodynamic properties of crystals [26]. Implicit in Eq. (20) is the assumption that the distribution is identical about every site of the solid. While rigorously true of the Bravais lattices, this assumption is not strictly valid for the other structures considered. Although, in principle, a different variational width parameter could be assigned to each distinct site, or even free minimization could be performed [47], in practice the associated numerical cost of multi-dimensional minimization would make prohibitive such an extensive survey of pair potentials, solid structures, and thermodynamic states as we undertake here. In any case, excepting the most open structures, the density distribution is expected to be isotropic and Gaussian to within a reasonable approximation, as discussed in Sec. V. Thus, all of our free energy calculations make use of the Gaussian ansatz (20).

The density of any periodic solid may be represented as a Fourier series of the general form

$$\rho(\mathbf{r}) = \frac{1}{V} \sum_{\mathbf{G}} \rho_{\mathbf{G}} e^{i\mathbf{G}\cdot\mathbf{r}}, \quad (21)$$

where V is the total volume and the sum is over the reciprocal lattice vectors (RLV) \mathbf{G} of the underlying Bravais lattice. For the density defined by Eq. (20), the Fourier transform of $\rho(\mathbf{r})$ may be factorized as

$$\rho_{\mathbf{G}} \equiv \int d\mathbf{r} e^{-i\mathbf{G}\cdot\mathbf{r}} \rho(\mathbf{r}) = N \exp(-G^2/4\alpha) S_{\mathbf{G}}, \quad (22)$$

where

$$S_{\mathbf{G}} = \frac{1}{N_b} \sum_{\mathbf{d}} e^{-i\mathbf{G}\cdot\mathbf{d}} \quad (23)$$

is a geometrical structure factor and N_b is the number of basis atoms. Substituting Eqs. (21) and (22) into Eq. (15), the weighted density in the MWDA may then be expressed in the form

$$\hat{\rho} = \rho_s \left[1 + \sum_{G \neq 0} \exp(-G^2/2\alpha) w_G \sum_{\text{deg}} |S_{\mathbf{G}}|^2 \right], \quad (24)$$

with $\rho_s \equiv N/V$ being the average solid density, w_G the Fourier transform of the weight function, and where we have used the property $S_{-\mathbf{G}} = S_{\mathbf{G}}^*$. The first sum in Eq. (24) is over magnitudes of the RLV's, and the second is over degeneracies, that is, over all RLV's having the same magnitude G . Note that for a given structure, the latter sum need be computed only once for each magnitude G (most efficiently in complex arithmetic). Computation of $\hat{\rho}$ via Eq. (24) is now achieved by a straightforward summation over RLV magnitudes, and substitution into Eq. (14) then immediately gives the HS reference excess free energy [first term on right side of Eq. (19)].

For density distributions sufficiently narrow that neighboring Gaussians do not significantly overlap, the ideal-gas free energy per particle [Eq. (6)] is very accurately approximated by

$$F_{id}/N = \frac{3}{2}k_B T \ln(\alpha\lambda^2), \quad (25)$$

to within an irrelevant additive constant. Typically, Eq. (25) is valid for $\alpha d^2 > 50$, a condition always satisfied at the densities of interest here.

The perturbation free energy [second term on right side of Eq. (19)] is similarly computed in Fourier space by first rewriting it in the form

$$F_p[\rho; d] = \frac{1}{2} \int d\mathbf{r} \int d\mathbf{r}' \rho(\mathbf{r})\rho(\mathbf{r}') [\phi_p(|\mathbf{r} - \mathbf{r}'|) + \phi_p(d)\theta(|\mathbf{r} - \mathbf{r}'| - d)], \quad (26)$$

where θ denotes the Mayer function for hard spheres, defined by $\theta(x) \equiv u(x) - 1$. The Fourier space representation is then easily shown to be

$$F_p[\rho; d]/N = \frac{1}{2}\rho_s \sum_G \exp(-G^2/2\alpha) [\tilde{\phi}_p(G) + \phi_p(d)\tilde{\theta}(G)] \sum_{\text{deg}} |S_{\mathbf{G}}|^2, \quad (27)$$

where

$$\tilde{\phi}_p(G) \equiv \int d\mathbf{r} e^{-i\mathbf{G}\cdot\mathbf{r}} \phi_p(r) \quad (28)$$

is the Fourier transform of the perturbation potential, and

$$\tilde{\theta}(G) \equiv \int d\mathbf{r} e^{-i\mathbf{G}\cdot\mathbf{r}} \theta(r - d) = -\frac{4\pi}{G^3} [\sin(Gd) - Gd \cos(Gd)]. \quad (29)$$

In practice, $\tilde{\phi}_p(G)$ is readily computed by a fast Fourier transform algorithm. Care must be taken to sum Eqs. (24) and (27) over a sufficiently high number of RLV's to ensure convergence.

For fixed ρ_s , T , and pseudopotential parameters Z and r_c , the free energy functional is computed from Eqs. (14), (19), (24), (25), and (27) for a given solid structure and then minimized with respect to α to obtain the free energy. For the hcp crystal, additional minimization with respect to the c/a ratio is performed. The existence of a variational minimum implies that the chosen solid is at least mechanically stable. Finally, comparing the free energies of different solid structures and of the liquid, the thermodynamically stable structure is determined as that having the lowest free energy.

IV. SURVEY OF RELATIVE STABILITIES

A. Quasicrystal Structural Model

The quasicrystalline structure is modelled here by a three-dimensional Penrose tiling constructed by the projection of a six-dimensional hypercubic lattice onto the three-dimensional physical space, such that the six hypercubic basis vectors are projected onto six vectors forming an icosahedral basis

$$\{\mathbf{e}_i; i = 1, \dots, 6\} = c\{(1, \tau, 0) + \text{cyclic permutations (c.p.); } (-1, \tau, 0) + \text{c.p.}\}, \quad (30)$$

with $c = (1 + \tau^2)^{-1/2} = (2 + \tau)^{-1/2}$, where $\tau = (1 + \sqrt{5})/2$ is the golden mean. To each of the basis vectors \mathbf{e}_i there corresponds in the three-dimensional space orthogonal to the physical space a basis vector

$$\{\mathbf{e}_i^\perp; i = 1, \dots, 6\} = c\{(-\tau, 1, 0) + \text{c.p.}; (\tau, 1, 0) + \text{c.p.}\}. \quad (31)$$

The Penrose lattice consists of all points whose images in six dimensions lie inside an acceptance domain V_A^\perp with the form of a rhombic triacontahedron described by

$$V_A^\perp \equiv \{\mathbf{x}_o^\perp + \sum_{i=1}^6 \xi_i \cdot \mathbf{e}_i^\perp; 0 \leq \xi_i \leq 1\}. \quad (32)$$

The basic units of the Penrose lattice are prolate and oblate rhombohedra spanned by the basis vectors $(\mathbf{e}_1, \mathbf{e}_5, \mathbf{e}_6)$ and $(\mathbf{e}_2, \mathbf{e}_5, \mathbf{e}_6)$, respectively. If all vertices of a Penrose lattice are occupied by atoms, three types of bonds can be distinguished: *a*-bonds along the edge of the rhombohedra, *b*-bonds of length $1.05a$ along the short diagonal of a rhombic face, and *c*-bonds of length $0.56a$ along the short body diagonal of the oblate rhombohedra. Note that second-nearest neighbors connected via two *c*-bonds appear at a distance of $1.12a$. The existence of the short *c*-bonds limits the diameters of the atoms that can be placed on the vertices and leads to a very low packing fraction. In the “unit-sphere packing” on a Penrose lattice proposed by Henley [49], a more compact structure is achieved by occupying only one of the sites on both ends of a *c*-bond. Since there is no essential asymmetry between

these two sites, the choice of the empty sites is subject to some degree of arbitrariness. The choice is unique only in the case of c -bonds forming chains with an even number of members: in this case the end-points and every second point along the chain are occupied. Except for a small number of end-points of c -chains, the empty sites have four a -, five b -, and two c -bonds, and are surrounded by two oblate and two prolate rhombohedra forming together a rhombic dodecahedron. From the frequency of the dodecahedra, the average occupancy of the vertices of the Penrose lattice can be estimated as 0.7802 (for further details, see Henley [49]), leading to a maximum packing fraction for the hard-sphere quasicrystal of $\eta_{QC} = 0.6288$, rather close to the highest achievable packing fraction for a random packing of hard spheres, $\eta_{RPHS} = 0.636$. (The maximum packing fraction, defined as the volume ratio, with respect to the total volume, of tightly packed hard spheres, provides a standard measure of packing efficiency.)

The elimination of a specific class of lattice sites from the Penrose tiling creates a certain complication: if the images of the empty sites are eliminated from the acceptance domain V_A^\perp , a non-compact multiply-connected domain is formed. As a consequence, techniques for performing real and reciprocal quasi-lattice sums based on integrations over the acceptance domain in perpendicular space are not easily applicable to the unit-sphere packing. A way out of the dilemma is to perform the calculations for a hierarchy of rational approximants coming arbitrarily close to the quasiperiodic limit. A rational approximant is a periodic structure that is obtained if, in the icosahedral basis in perpendicular space $\{\mathbf{e}_i^\perp\}$, the golden mean τ is replaced by a rational number $\tau_n = F_{n+1}/F_n$, where F_n is a Fibonacci number defined by the recursive relation $F_{n+1} = F_n + F_{n-1}$, with $F_0 = F_1 = 1$. As an approximant is simply a crystal with a large unit cell, conventional techniques for performing lattice sums can be applied. Table I lists the number of basis atoms N_b in the periodically repeated unit cell and the maximum packing fraction η_m for the first four generations of approximant to the quasiperiodic unit-sphere packing. Note that for the fourth-order approximant η_m is already very close to the quasiperiodic limit, and that all of the approximants have maximum packing fractions lower than those of the crystals examined. For a more detailed discussion

of rational approximants to the Penrose lattice see, *e.g.*, Krajčí and Hafner [50].

For comparison with previous studies, we note that the lattice-sum calculations of Smith [6] were performed on quasicrystal structures with various compact non-convex acceptance domains selected so as to maximize the packing fraction. The most compact packing is achieved for an acceptance domain in the form of a “truncated stellated dodecahedron” (TSD) ($\eta_{TSD} = 0.628$). Only this type of quasicrystal was found to be more stable than the tested crystalline structures in a certain range of parameter space (valence, pseudopotential core radius, and atomic volume). The DF study of M^cCarley and Ashcroft [9], for a system of hard spheres, also found the TSD acceptance domain to produce the most stable quasicrystal, although for that system only metastable. The lattice-sum calculations of Windisch [7], on the other hand, dealt directly with the same rational approximants to the quasicrystalline unit-sphere packing that we examine here by DF theory.

B. Results and Discussion

As a simple but essential test of the theory, we first apply it to the hard-sphere reference system alone. Figure 2 shows the predicted free energy per volume (in thermal units) as a function of average density for the various solid structures discussed above, as well as for the HS fluid. (Note that, because of the infinitely steep repulsion of the HS potential at contact, the free energy has only a trivial linear temperature dependence, *i.e.*, $F/k_B T$ is independent of T .) At lower densities ($\rho\sigma^3 < 0.91$) the fluid phase is thermodynamically stable, while at higher densities ($\rho\sigma^3 > 1.04$) the close-packed crystals become inevitably stable. The fcc and hcp crystals are found to be essentially degenerate – within the presumed accuracy of the theory – consistent with simulation results, the minimizing hcp c/a ratio increasing gradually over the displayed density range from 1.633 (very close to the ideal value of $\sqrt{8/3}$) to 1.673. The bcc crystal – constrained by the density parametrization to be stable against shear – becomes more stable than the fluid at higher densities, but remains metastable relative to the close-packed crystals. Interestingly, the rational approximants are mechanically stable

over a comparatively wide range of densities, including lower densities where the crystals are unstable. The essential reason is that their density distributions are narrower than those of the crystals at the same average density (see below). Evidently, however, they remain metastable relative to both the fluid and the crystals. Furthermore, at a given density, their free energies decrease in order of increasing maximum packing fraction (cf. Table I), clearly demonstrating that the purely entropic HS system overwhelmingly favors packing efficiency. It is interesting to compare these results with those from a similar calculation, based on the same functional, for a HS glass [51]. For the random close-packed (RCP) model, the glass was found to be always metastable with respect to the fluid for $\eta_{RCP} < 0.672$, which is significantly above the maximum approximant packing fraction.

As a further test, we have applied the full perturbation theory to a system of rare gas atoms interacting via the Lennard-Jones (LJ) pair potential, a standard model that includes both short-range repulsive and long-range attractive interactions. In comparison with the results for the HS system, the qualitative picture is unchanged. The theory predicts the close-packed crystals to form the stable high-density phase, in agreement with simulations, and the rational approximants to be always at best metastable. The clear implication is that long-range attractive interactions are not, by themselves, sufficient to stabilize quasicrystalline structures.

As a final test of the theory, as well as of the pseudopotential approach outlined in Sec. II, we have examined the freezing transitions of two simple metallic elements, Mg ($Z = 2$, $r_c = 1.31a_o$) and Al ($Z = 3$, $r_c = 1.11a_o$). For both metals, the theory predicts coexisting liquid and solid densities and structural energy differences in reasonable agreement with experiment. Furthermore, for Mg it predicts hcp to be the stable equilibrium structure, while for Al it predicts fcc, consistent with observation. Details of this study will be presented elsewhere [37].

With reasonable grounds for confidence in the predictive power of the theory, we now proceed to a broad (and more ambitious) survey of the simple metals. Tables II-IV summarize our results over a range of pseudopotential parameters, $2.0 \leq Z \leq 3.4$ and

$0.400 \leq r_c/r_s \leq 0.575$. Note that although Z is of course an integer for any of the elements, we treat it here as a continuous parameter so as to better study trends in relative stabilities. The thermodynamic states represented are defined by fixed temperature $T = 500K$ and atomic volume (or average solid density) $\Omega = 120a_o^3$ ($\rho_s = 0.0562\text{\AA}^{-3}$), $\Omega = 150a_o^3$ ($\rho_s = 0.0450\text{\AA}^{-3}$), and $\Omega = 180a_o^3$ ($\rho_s = 0.0375\text{\AA}^{-3}$), for Tables II-IV, respectively. Tabulated for each parameter set are, from top to bottom: (*i*) the most stable structure, of the liquid and the seven solids tested, determined as that having the lowest free energy (structures in parentheses being metastable with respect to the liquid); (*ii*) the corresponding Lindemann ratio L , defined as the ratio of the root-mean-square atomic displacement (away from the equilibrium site) to the nearest-neighbor distance, and given in the Gaussian approximation [Eq. (20)] by

$$L = \left(\frac{3}{2\alpha}\right)^{1/2} / \left(\frac{6}{\pi}\Omega\eta_m\right)^{1/3}, \quad (33)$$

α being the minimizing Gaussian width parameter; and (*iii*) the effective HS diameter d , computed from Eq. (13).

Tables II-IV are dense with information. For purposes of orientation, we note that hcp-Mg occurs at $r_c/r_s = 0.539, 0.501,$ and 0.471 , corresponding to compressed, near-equilibrium, and expanded states, respectively. Similarly, expanded fcc-Al would occur at $r_c/r_s = 0.523, 0.486,$ and 0.457 , were it not that at such low densities the fcc crystal is unstable (see below). Physical interpretation is greatly aided by considering the effective HS packing fraction, defined by $\eta \equiv \frac{\pi}{6}\rho d^3$. By default, the liquid is considered the stable phase when η is so low that none of the solid structures is stable against thermally induced atomic displacements. (The states considered are well removed from the vapour phase.) At sufficiently high η , the close-packed fcc and hcp crystals tend to be thermodynamically stable, the minimizing hcp c/a ratio lying close to, although usually slightly above, the ideal ratio. This is to be expected, since experience with the HS system indicates that strongly repulsive short-range interactions heavily favor packing efficiency. In contrast to the HS and LJ systems, the fcc and hcp free energies are generally sufficiently different to clearly distinguish

their relative stabilities, reflecting some influence of longer-range interactions. The more open bcc structure is always at best metastable, and thus appears nowhere in the stability tables. In these qualitative respects, the simple metals do not differ significantly from the HS and LJ systems. Remarkably, however, in a relatively narrow band of parameter space, corresponding to intermediate effective packings, the rational approximants are predicted to be metastable or, in some cases, even *thermodynamically* stable. Although this parameter range contains none of the elements from the Periodic Table, we note that it does include the virtual-crystal parameters (average densities, valences, and core radii) characteristic of some of the known multi-component s,p-bonded quasicrystals, *e.g.*, Al-Mg-Li, Al(Ga)-Mg-Zn, and Al-Li(Mg)-Cu. However, since these ternary alloys are composed of elements with atomic size ratios rather far from unity, the relevance of the simple virtual-crystal approximation must be considered doubtful. Clearly, the size disparity of constituent elements constitutes an important element in the discussion of structural stabilities of alloys. This issue may be addressed by future extension of the DF approach to multi-component metallic systems, for which purpose a generalization of the MWDA to binary HS mixtures [52] may prove useful.

We now turn to the physical reasons underlying the predicted thermodynamic stability of quasicrystalline structures. When the effective HS packing fraction is sufficiently low that the free energy functional has no variational minimum, the solid exhibits what we term a *phonon instability*. Such unstable regions in the parameter space of Tables II-IV are readily explained by considering trends in the effective HS diameter. In general, d is seen to decrease with increasing valence (across a row) and with decreasing core radius (down a column), in line with previous remarks regarding the core region of the pair potential (see Sec. II). Correspondingly, the atoms in the solid become more loosely packed and their density distributions broader, as reflected by the increasing Lindemann ratio for a given structure. Ultimately, when $L > 0.10 - 0.15$ the atomic packing becomes so loose that the solid – whatever its structure – is no longer stable against vibrational displacements of the atoms away from their equilibrium sites (phonons). The theory is thus consistent with the Lindemann criterion for melting, according to which a solid becomes unstable when

atomic displacements exceed roughly 10% of the nearest-neighbor distance. Significantly, the rational approximants, despite being less efficiently packed (and thus having shorter nearest-neighbor distances) than the crystals, have consistently smaller Lindemann ratios. This implies greater vibrational stiffness, which tends to enhance their structural stability over that of the crystals. In passing, we note that this may be related to certain mechanical and transport properties characteristic of many quasicrystals, such as high brittleness and low electrical and thermal conductivities. The phonon instability partly explains the appearance of the rational approximants near the table diagonals, where the crystals lose mechanical stability, and the absence of any stable structure towards the lower-right corner of the tables. It also accounts for the 1/1 metastability along the entire bottom row of Table IV, where all other structures are mechanically unstable.

Where no entries are given in the stability tables, the free energy cannot be evaluated within the theory for any of the structures considered. The reason is revealed by closer inspection of the effective HS diameter. In exception to the above-noted trend, d can be anomalously large when the electron density is sufficiently high and r_c sufficiently small. Comparison with the pair potentials in Fig. 1 shows that this inflation of the effective hard core occurs precisely when the first minimum of the Friedel oscillations happens to lie beneath the core, inducing a repulsive shoulder and pushing the first minimum of the pair potential out to larger distances. [Compare, for example, the diameter in Table II at $Z = 3.2$, $r_c/r_s = 0.5$ with its counterpart pair potential in Fig. 1 (a).] When d is so large, and Ω so small, that the maximum HS packing fraction of a given solid structure (Table I) is exceeded, the repulsive core regions of nearest-neighbor atoms overlap at equilibrium separation. Such an energetically unfavorable configuration exhibits what we term a *packing instability*. In such cases, it proves impossible to find a self-consistent solution for the weighted density [Eq. (24)]. The theory thus appropriately forbids such unphysical states. Packing instability is a second reason for the loss of structural stability upon approaching the lower-right corner of Tables II-IV, particularly at lower atomic volumes. Of course there is some degree of arbitrariness in splitting the effective pair potential at the first, rather than the second,

minimum. We note that at $T = 500$ K the characteristic thermal energy $k_B T \simeq 3$ mRy is comparable to the barrier height, which justifies our choice of convention. For shouldered potentials, however, the size of the effective hard core may be artificially inflated, resulting in a possible underestimate of quasicrystalline stability, particularly at higher densities.

The analysis of structural trends across the Periodic Table [17], as well as lattice-sum calculations [6,7] for a wide variety of crystal structures have shown that if the effective pair potential develops a shoulder at a distance close to the nearest-neighbor separation in a close-packed structure, a lattice distortion or finally the formation of a more open crystal structure becomes energetically favorable. Characteristic examples falling within the parameter range covered by this study are the rhombohedral structure of Hg ($Z = 2$, $r_c/r_s \leq 0.40$) and the orthorhombic structure of α -Ga ($Z = 3$, $r_c/r_s \leq 0.48$). At even higher valence, the same effect explains the transition from close-packed metallic to open covalent structures. Covalency also entails three- and many-body forces, which are necessary to ensure the dynamic stability of the open structures. Many-body forces, however, are clearly outside the scope of current pseudopotential and DF theories.

To this point, we have explained the loss of mechanical stability in terms of phonon and packing instabilities. Physical insight into the source of thermodynamic stability is gained by examining separately the reference and perturbation contributions to the total free energy. The reference free energy combines the entropy and that part of the internal energy that derives from short-range interactions, while the perturbation free energy is the remaining part of the internal energy deriving from medium- and long-range interactions. Figure 3 compares the reference and perturbation free energies of the various structures as a function of Z for fixed chosen values of r_c/r_s and Ω . We emphasize that because of the ignored volume term (see Sec. III) only free energy *differences* are physically relevant. That the reference free energy consistently favors the close-packed crystals is to be expected, since the reference system here is a HS solid. More revealing is that the perturbation free energy, although reinforcing the stability of the compact crystals at lower Z , increasingly disfavors them relative to the more open quasicrystals as Z increases. This can be largely understood

by noting that at lower Z , where the Friedel oscillations are longer in wavelength, the first minimum of $\phi(r)$ is relatively deep and coincides closely with the first nearest-neighbor distances of the highly-coordinated fcc and hcp structures. With increasing Z , however, as the Friedel oscillations shorten in wavelength and move under the repulsive core, the first minimum becomes shallower and shifts to shorter distances more commensurate with the first nearest-neighbor distances of the rational approximant structures (cf. the discussion of relative stabilities of crystalline structures given by Hafner and Heine (1983) [17]). Thus the oscillating part of the effective pair potential clearly emerges as the source of thermodynamic stability of simple metallic quasicrystals. The actual order of stabilities depends on a detailed competition between reference and perturbation free energies or, equivalently, between strongly repulsive short-range and weaker medium-long-range interactions.

The issue of structural stability may be framed alternatively in terms of a competition between internal energy U and entropy S . (For clarity, it should be noted that we do not consider here the role of phason entropy, since construction of the rational approximants does not involve the breaking of any matching rules.) Whereas in the lattice-sum method [6,7] only U is calculated, in the DF approach both U and S may be separated from the free energy via the thermodynamic relations

$$U = F + TS \tag{34}$$

and

$$S = - \left(\frac{\partial F}{\partial T} \right)_\rho \tag{35}$$

We have numerically performed the separation and individually compared the resulting U and S for the different structures. We find in this way that entropy tends to favor the periodic crystals, whereas internal energy tends to favor the rational approximants. These tendencies, however, are not as decisive as those exhibited by the reference and perturbation free energies, respectively. Thus, our DF-perturbation theory approach demonstrates the utility of interpreting relative structural stabilities in terms of a competition between short-

and medium-long-range interactions, as an alternative to the more conventional comparison of energy and entropy. Furthermore, it indicates that even though entropic effects tend to favor close-packed structures, internal energy associated with longer-range interactions may still prevail in stabilizing quasicrystallinity.

Finally, we consider the temperature dependence of the relative stabilities. For an effective pair potential corresponding to a point near the diagonal of Table III, Fig. 4 displays the free energy per particle as a function of temperature, at fixed average density, for three rational approximants ($1/1$ is unstable here) and for the liquid. Because the zero of the vertical scale is arbitrary, only free energy differences are physically meaningful. With decreasing temperature, one observes an inevitable liquid-solid transition. More interesting is that for this case a distinct cross-over in stability occurs between the different approximants. At higher temperatures, where short-range repulsive interactions dominate structural stability, the more efficiently packed short-period $2/1$ structure is most stable (though metastable relative to the liquid). At lower temperatures, medium- and long-range forces become more significant, ultimately stabilizing the long-period $5/3$ structure.

V. SUMMARY AND CONCLUSIONS

Summarizing, we have applied a density-functional-based perturbation theory to the question of the thermodynamic stability of one-component crystals and rational approximant models of quasicrystals, interacting via effective metallic pair potentials derived from pseudopotential theory. The theory is based on a splitting of the pair potential into a strongly repulsive short-range part and a relatively weak oscillating tail and the variational minimization of an approximate free energy functional with respect to the Gaussian-parametrized density distribution. Comparing the free energies of several plausible solid structures over a range of pseudopotential parameters and thermodynamic states corresponding to simple metals, we have identified general trends in relative stabilities. With increasing electronic valence and decreasing core radius, the solid becomes increasingly unstable towards atomic

displacements as the atoms become more loosely packed. Near electronic valences and core radii for which the close-packed crystals lose mechanical stability, the theory predicts thermodynamic stability of the vibrationally stiffer quasicrystalline structures.

Some limitations of the theory should be emphasized. First, the DF approach, because it requires prior specification of the solid structure, cannot by itself predict the globally stable symmetry. It can, however, predict the relative stabilities of a set of prescribed structures. Although our survey includes several of the more likely structures, it is conceivable that others not examined, or not treatable by the theory, may prove to be more stable. In particular, DF theory cannot describe freezing into the more open crystal structures (*e.g.*, α, γ -Hg, α -Ga, α, β -Sn) appearing close to the transition from metals to semimetals and semiconductors. In these materials, the liquid is always more metallic than the solid, violating a basic assumption of DF theory that the interatomic potentials do not change at the transition. The important point, however, is that in the lower-right half of Tables II-IV the stability of the quasicrystalline structures will be limited by the higher stability of comparatively open and at least partially covalent structures. We can locate the transition by drawing a line between the points representing Hg and Ga. This line coincides approximately with the limits of stability of the quasicrystalline approximants (again in good agreement with the lattice-sum calculations). Hence, our conclusions are not affected by this limitation.

Second, convergence of the perturbation expansion at first-order [Eq. 8] is not ensured down to arbitrarily low temperatures. In principle, convergence can be established by comparing the first-order contribution with the residual contribution due to neglected higher-order terms. (Note that the relative magnitudes of reference and perturbation free energies do not necessarily reflect the degree of convergence.) Of course in practice, the higher-order terms are unknown. As noted in Sec. III A, however, they are proportional to fluctuations in the total perturbation energy and to successively higher powers of $1/k_B T$. In general, if the change in $\phi_p(r)$ relative to $k_B T$ is sufficiently small over distances within which the single-particle density of the solid (or radial distribution function of the liquid) is significant, then these terms can be safely neglected. For the temperatures and average densities of interest

here, the solid density distributions (and peaks in the liquid radial distribution functions) are so narrow that the first-order approximation is expected to be rather accurate. As a typical example, consider the case of Fig. 1a for $Z = 2.6$. From Table II, at $T = 500K$ the stable structure is the fcc crystal with Lindemann ratio $L = 0.101$. The variation of $\phi_p(r)$ at the nearest-neighbor distance $r_{nn} \simeq 5.54a_o$ over the relevant distance $r_{nn}L$ is considerably smaller than $k_B T \simeq 3$ mRy, indicating good convergence. Caution is naturally advised, however, in extension of the first-order approximation to significantly lower temperatures.

Third, the assumption of a single-parameter isotropic Gaussian density distribution is certainly of restricted validity, especially for very anisotropic structures. The close-packed crystals are known to be reasonably isotropic and Gaussian [46,47]. For the relatively open eight-fold coordinated bcc crystal, on the other hand, the isotropic assumption should not be particularly accurate, especially near the melting transition. Quasicrystals and their higher-order approximants, however, are known to be elastically isotropic [53] and also to exhibit isotropic dispersion relations of acoustic phonons [54]. Furthermore, their relatively narrow density distributions (small Lindemann ratios) tend to minimize the significance of any deviations from Gaussian form. Hence, an isotropic Gaussian distribution should be rather accurate for these structures. In any case, the incorporation of additional degrees of freedom into a more flexible and realistic density parametrization would only result in *increasing* the stability of the rational approximants. Such technical refinements to the theory therefore should not qualitatively change our conclusions.

Lattice-sum studies [6,7], based on ground-state energy calculations, gave the first intriguing indication of *energetically* stable one-component metallic quasicrystals at zero temperature, but left open the issue of thermodynamic stability at finite temperatures. Previous DF studies of hard-sphere systems [9,10] effectively ruled out vibrational and configurational entropy as the source of quasicrystal stability, but did not consider the role of longer-range interactions. Using a practical DF-perturbation approach, we have now directly addressed these issues, and in the process demonstrated that the remarkable lattice-sum predictions carry over to finite temperatures. Furthermore, our approach yields new physical insight by

explaining the stability of quasicrystals in terms of their enhanced vibrational stiffness and the stabilizing influence of medium- and long-range interactions.

ACKNOWLEDGMENTS

We thank G. Kahl for numerous helpful discussions and M. Krajčí and M. Windisch for valuable assistance with the rational approximant structures. This work was supported by the Fonds zur Förderung der wissenschaftlichen Forschung (Austrian Science Foundation) to whom one of us (ARD) is grateful for a Lise-Meitner Fellowship.

* Present address: Institut für Festkörperforschung, Forschungszentrum Jülich GmbH, D-52425 Jülich, Germany (e-mail: a.denton@kfa-juelich.de)

REFERENCES

- [1] D. Shechtman, I. Blech, D. Gratias, and J.W. Cahn, Phys. Rev. Lett. **53**, 1951 (1984).
- [2] C. Janot, *Quasicrystals* (Clarendon, Oxford, 1992).
- [3] P.J. Steinhardt and D.P. DiVincenzo (editors), *Quasicrystals: The State of the Art* (World Scientific, Singapore, 1991).
- [4] A.-P. Tsai, A. Inoue, and T. Masumoto, Jap. J. Appl. Phys. **26**, L1505 (1987).
- [5] S. Narasimhan and M. Jarić, Phys. Rev. Lett. **62**, 454 (1989).
- [6] A.P. Smith, Phys. Rev. B **43**, 11635 (1991); Phys. Rev. B **42**, 1189 (1990); A.P. Smith and N.W. Ashcroft, Phys. Rev. B **38**, 12942 (1988).
- [7] M. Windisch, *Diplomarbeit* (Technische Universität Wien, 1991).
- [8] R. Evans, in *Inhomogeneous Fluids*, edited by D. Henderson (Dekker, 1992); D.W. Oxtoby, in *Liquids, Freezing, and Glass Transition*, Les Houches session 51, edited by J.-P. Hansen, D. Levesque, and J. Zinn-Justin (North-Holland, Amsterdam, 1991).
- [9] J.S. McCarley and N.W. Ashcroft, Phys. Rev. B **49**, 15600 (1994).
- [10] M. Popović and M. Jarić, Phys. Rev. B **38**, 808 (1988).
- [11] R.O. Jones and O. Gunnarsson, Rev. Mod. Phys. **61**, 689 (1989).
- [12] N.W. Ashcroft and D. Stroud, Solid State Phys. **33**, 1 (1978).
- [13] J.-P. Hansen and I.R. McDonald, *Theory of Simple Liquids*, 2nd edition (Academic, London, 1986).
- [14] W.A. Harrison, *Pseudopotentials in the Theory of Metals* (Benjamin, New York, 1970).
- [15] V. Heine, Solid State Phys. **24**, 1 (1970).
- [16] J. Hafner, *From Hamiltonians to Phase Diagrams* (Springer, Berlin, 1987).

- [17] J. Hafner and V. Heine, *J. Phys. F: Met. Phys.* **13**, 2479 (1983); **16**, 1429 (1986).
- [18] S. Ichimaru and K. Utsumi, *Phys. Rev. B* **24**, 7385 (1981).
- [19] N.W. Ashcroft, *Phys. Lett.* **23**, 48 (1966).
- [20] N.D. Mermin, *Phys. Rev.* **137**, A1441 (1965).
- [21] R. Evans, *Adv. Phys.* **28**, 143 (1979).
- [22] P. Tarazona, *Mol. Phys.* **52**, 81 (1984); **61**, 798 (1987) (erratum); P. Tarazona, *Phys. Rev. A* **31**, 2672 (1985).
- [23] W.A. Curtin and N.W. Ashcroft, *Phys. Rev. A* **32**, 2909 (1985).
- [24] W.A. Curtin and N.W. Ashcroft, *Phys. Rev. Lett.* **56**, 2775 (1986); **57**, 1192 (1986) (erratum).
- [25] R.S. Jones and N.W. Ashcroft, *J. Chem. Phys.* **80**, 3328 (1984).
- [26] H. Löwen, *Phys. Reports* **237**, 249 (1994); Y. Singh, *Phys. Reports* **207**, 351 (1991).
- [27] D.W. Oxtoby, *J. Chem. Phys.* **76**, 6262 (1982).
- [28] F. Igloi, G. Kahl, and J. Hafner, *J. Phys. C: Solid State Phys.* **20**, 1803 (1987).
- [29] B.B. Laird and D.M. Kroll, *Phys. Rev. A* **42**, 4810 (1990).
- [30] A. Kyrilidis and R.A. Brown, *Phys. Rev. A* **44**, 8141 (1991).
- [31] M. Hasegawa, *J. Phys. Soc. Japan* **62**, 4316 (1993).
- [32] J.D. Weeks, D. Chandler, and H.C. Andersen, *J. Chem. Phys.* **54**, 5237 (1971).
- [33] A. Kyrilidis and R.A. Brown, *Phys. Rev. E* **47**, 427 (1993).
- [34] L. Mederos, G. Navascués, P. Tarazona, and E. Chacón, *Phys. Rev. E* **47**, 4284 (1993);
L. Mederos, G. Navascués, and P. Tarazona, *Phys. Rev. E* **49**, 2161 (1994).

- [35] J. Hafner, Phys. Rev. A **16**, 351 (1977).
- [36] J. Hafner and G. Kahl, J. Phys. F: Met. Phys. **14**, 2259 (1984).
- [37] A.R. Denton, J. Hafner and G. Kahl (unpublished).
- [38] R. Zwanzig, J. Chem. Phys. **22**, 1420 (1954).
- [39] A.R. Denton and N.W. Ashcroft, Phys. Rev. A **39**, 4701 (1989).
- [40] J.J. Weis, Mol. Phys. **28**, 187 (1974); J.M. Kincaid and J.J. Weis, Mol. Phys. **34**, 931 (1977); H.S. Kang, T. Ree, and F.H. Ree, J. Chem. Phys. **84**, 4547 (1986); Y. Choi, T. Ree, and F.H. Ree, J. Chem. Phys. **95**, 7548 (1991).
- [41] W.A. Curtin, Phys. Rev. B **39**, 6775 (1989).
- [42] C.N. Likos, Zs. Németh, and H. Löwen, J. Phys.: Condens. Matter **6**, 10965 (1994).
- [43] A.R. Denton and H. Löwen, J. Phys.: Condens. Matter **9**, L1 (1997).
- [44] A.I. Goldman and R.F. Kelton, Rev. Mod. Phys. **65**, 213 (1993).
- [45] N.W. Ashcroft and N.D. Mermin, *Solid State Physics* (Holt, Rinehart and Winston, Philadelphia, 1976).
- [46] D.A. Young and B.J. Alder, J. Chem. Phys. **60** 1254 (1974).
- [47] R. Ohnesorge, H. Löwen, and H. Wagner, Europhys. Lett. **22** 245 (1993).
- [48] B.B. Laird, J.D. McCoy, and A.D.J. Haymet, J. Chem. Phys. **87** 5449 (1987).
- [49] C.L. Henley, Phys. Rev. B **34**, 797 (1986).
- [50] M. Krajčí and J. Hafner, Phys. Rev. B **46**, 10669 (1992).
- [51] H. Löwen, J. Phys.: Condens. Matter **2**, 8477 (1990).
- [52] A.R. Denton and N.W. Ashcroft, Phys. Rev. A **42**, 7312 (1990).

- [53] T.C. Lubensky, J.E.S. Socolar, P.J. Steinhardt, P.A. Bancee, and P.A. Heiney, Phys. Rev. Lett. **57**, 1440 (1986).
- [54] J. Hafner and M. Krajčí, J. Phys.: Condens. Matter **5**, 2489 (1993).

FIGURES

FIG. 1. Effective pair potentials for several pseudopotential parameters: (a) valence $Z = 2.0$ (solid curve), 2.6 (long-dashed), and 3.2 (short-dashed) for fixed ratio of core radius to electron-sphere radius $r_c/r_s = 0.50$ and atomic volume $\Omega = 120a_o^3$; (b) same as (a), but for $\Omega = 150a_o^3$; (c) $r_c/r_s = 0.40$ (solid), 0.45 (long-dashed), 0.50 (short-dashed), and 0.55 (dot-dashed) for fixed $Z = 3.0$ and $\Omega = 150a_o^3$. (See Tables II and III for corresponding effective hard-sphere diameters at $T = 500K$.)

FIG. 2. Free energy per unit volume (in thermal units) vs. average density of the hard-sphere reference system: Fluid (thick solid curve), fcc and hcp (thick long-dashed), bcc (thick short-dashed), 1/1 (thin dot-dashed), 2/1 (thin solid), 3/2 (thin long-dashed), and 5/3 (thin short-dashed).

FIG. 3. (a) Reference hard-sphere free energy, and (b) perturbation free energy, for designated solid structures as a function of valence Z at fixed core radius $r_c/r_s = 0.550$, atomic volume $\Omega = 150a_o^3$, and temperature $T = 500K$.

FIG. 4. Free energy per particle vs. temperature for the liquid (solid curve) and for the 2/1 (long-dashed), 3/2 (short-dashed), and 5/3 (dot-dashed) rational approximants at fixed atomic volume $\Omega = 150a_o^3$, valence $Z = 3.0$, and core radius $r_c/r_s = 0.500$.

TABLES

TABLE I. Number of basis atoms per unit cell and maximum packing fraction for the first four rational approximants to the unit-sphere packing model (see Sec. IV A) and three elementary crystals.

Structure	Basis Size	Maximum Packing Fraction
1/1	20	0.5020
2/1	108	0.6400
3/2	452	0.6323
5/3	1904	0.6287
fcc	1	0.7405
hcp	2	0.7405
bcc	1	0.6802

TABLE II. Thermodynamically stable structure, corresponding Lindemann ratio, and effective hard-sphere diameter d (in Bohr radii), at fixed atomic volume $\Omega = 120a_0^3$ and temperature $T = 500K$, over a range of pseudopotential parameters: valence Z and core radius r_c as a ratio of electron-sphere radius r_s . (Parentheses indicate metastability with respect to the liquid phase.)

r_c/r_s	Z							
	2.0	2.2	2.4	2.6	2.8	3.0	3.2	3.4
0.575	fcc	fcc	fcc	fcc	fcc	fcc	2/1	2/1
	0.00799	0.0220	0.0343	0.0441	0.0538	0.0676	0.0606	0.0763
	5.489	5.397	5.317	5.246	5.182	5.127	5.078	5.035
0.550	hcp	fcc	fcc	fcc	fcc	hcp	2/1	2/1
	0.0288	0.0366	0.0468	0.0565	0.0695	0.101	0.0762	0.0941
	5.389	5.308	5.235	5.173	5.117	5.070	5.031	4.999
0.525	hcp	fcc	fcc	fcc	fcc	2/1	2/1	2/1
	0.0397	0.0513	0.0610	0.0737	0.0952	0.0783	0.0934	0.107
	5.286	5.214	5.152	5.099	5.055	5.020	4.995	4.984
0.500	hcp	fcc	fcc	fcc	2/1	2/1	–	–
	0.0554	0.0678	0.0804	0.101	0.0829	0.0947	–	–
	5.176	5.116	5.067	5.027	4.999	4.986	6.972	6.939
0.475	hcp	fcc	fcc	2/1	–	–	–	–
	0.0767	0.0902	0.112	0.0909	–	–	–	–
	5.062	5.016	4.982	4.963	6.785	6.801	6.787	6.755
0.450	hcp	fcc	2/1	–	–	–	–	–
	0.105	0.129	0.104	–	–	–	–	–
	4.944	4.915	4.905	6.581	6.618	6.621	6.601	6.568
0.425	(2/1)	(2/1)	–	–	–	–	–	–
	0.111	0.127	–	–	–	–	–	–

	4.825	4.821	6.385	6.441	6.458	6.450	6.425	6.390
0.400	(5/3)	-	-	-	-	-	-	-
	0.149	-	-	-	-	-	-	-
	4.709	6.196	6.273	6.304	6.305	6.287	6.257	6.220

TABLE III. Same format as Table II, but for atomic volume $\Omega = 150a_o^3$.

r_c/r_s	Z							
	2.0	2.2	2.4	2.6	2.8	3.0	3.2	3.4
0.575	hcp	hcp	fcc	fcc	fcc	5/3	5/3	5/3
	0.0258	0.0285	0.0395	0.0450	0.0507	0.0453	0.0526	0.0631
	5.794	5.692	5.601	5.519	5.445	5.378	5.317	5.262
0.550	hcp	hcp	fcc	fcc	3/2	5/3	5/3	5/3
	0.0315	0.0356	0.0495	0.0554	0.0516	0.0581	0.0690	0.0876
	5.677	5.584	5.501	5.426	5.359	5.299	5.245	5.198
0.525	hcp	fcc	fcc	fcc	5/3	5/3	(5/3)	liquid
	0.0431	0.0558	0.0620	0.0706	0.0653	0.0771	0.0967	–
	5.553	5.470	5.395	5.329	5.271	5.219	5.174	5.135
0.500	hcp	fcc	fcc	(2/1)	(5/3)	(5/3)	liquid	liquid
	0.0625	0.0708	0.0802	0.0789	0.0878	0.109	–	–
	5.422	5.348	5.283	5.228	5.179	5.138	5.104	5.078
0.475	hcp	fcc	(fcc)	(2/1)	(3/2)	liquid	liquid	liquid
	0.0822	0.0931	0.113	0.110	0.135	–	–	–
	5.282	5.219	5.166	5.121	5.085	5.058	5.042	5.042
0.450	(hcp)	(fcc)	(2/1)	liquid	liquid	liquid	–	–
	0.111	0.137	0.134	–	–	–	–	–
	5.136	5.085	5.044	5.013	4.993	4.989	6.964	6.955
0.425	(2/1)	liquid	liquid	liquid	–	–	–	–
	0.131	–	–	–	–	–	–	–
	4.986	4.947	4.920	4.907	6.750	6.785	6.786	6.765
0.400	liquid	liquid	liquid	–	–	–	–	–
	–	–	–	–	–	–	–	–
	4.831	4.806	4.796	6.569	6.619	6.629	6.614	6.584

TABLE IV. Same format as Table II, but for atomic volume $\Omega = 180a_o^3$.

r_c/r_s	Z							
	2.0	2.2	2.4	2.6	2.8	3.0	3.2	3.4
0.575	hcp	hcp	fcc	fcc	5/3	5/3	5/3	5/3
	0.0256	0.0268	0.0426	0.0473	0.0395	0.0451	0.0520	0.0604
	6.065	5.953	5.853	5.763	5.682	5.607	5.539	5.477
0.550	hcp	hcp	fcc	fcc	5/3	5/3	(5/3)	(5/3)
	0.0315	0.0398	0.0522	0.0578	0.0513	0.0582	0.0670	0.0807
	5.934	5.831	5.739	5.656	5.581	5.513	5.451	5.394
0.525	hcp	fcc	fcc	5/3	5/3	(5/3)	(5/3)	(5/3)
	0.0502	0.0590	0.0647	0.0592	0.0663	0.0760	0.0919	0.129
	5.794	5.700	5.616	5.542	5.475	5.414	5.360	5.310
0.500	hcp	fcc	(fcc)	(5/3)	(5/3)	(5/3)	liquid	liquid
	0.0675	0.0740	0.0830	0.0770	0.0885	0.108	–	–
	5.644	5.561	5.486	5.420	5.362	5.310	5.263	5.224
0.475	hcp	(fcc)	(5/3)	(5/3)	(5/3)	liquid	liquid	liquid
	0.0865	0.0968	0.0908	0.106	0.134	–	–	–
	5.486	5.412	5.348	5.291	5.243	5.200	5.165	5.136
0.450	(hcp)	(fcc)	(5/3)	liquid	liquid	liquid	liquid	liquid
	0.116	0.140	0.130	–	–	–	–	–
	5.320	5.257	5.203	5.157	5.118	5.088	5.065	5.051
0.425	(2/1)	(1/1)	(1/1)	(1/1)	(1/1)	(1/1)	(1/1)	–
	0.141	0.0691	0.0758	0.0824	0.0886	0.0938	0.0970	–
	5.149	5.096	5.052	5.017	4.991	4.974	4.970	7.074
0.400	(1/1)	(1/1)	(1/1)	(1/1)	(1/1)	(1/1)	–	–
	0.0853	0.0929	0.101	0.109	0.115	0.117	–	–
	4.972	4.930	4.897	4.874	4.862	4.866	6.908	6.898

Fig. 1a (Denton and Hafner)

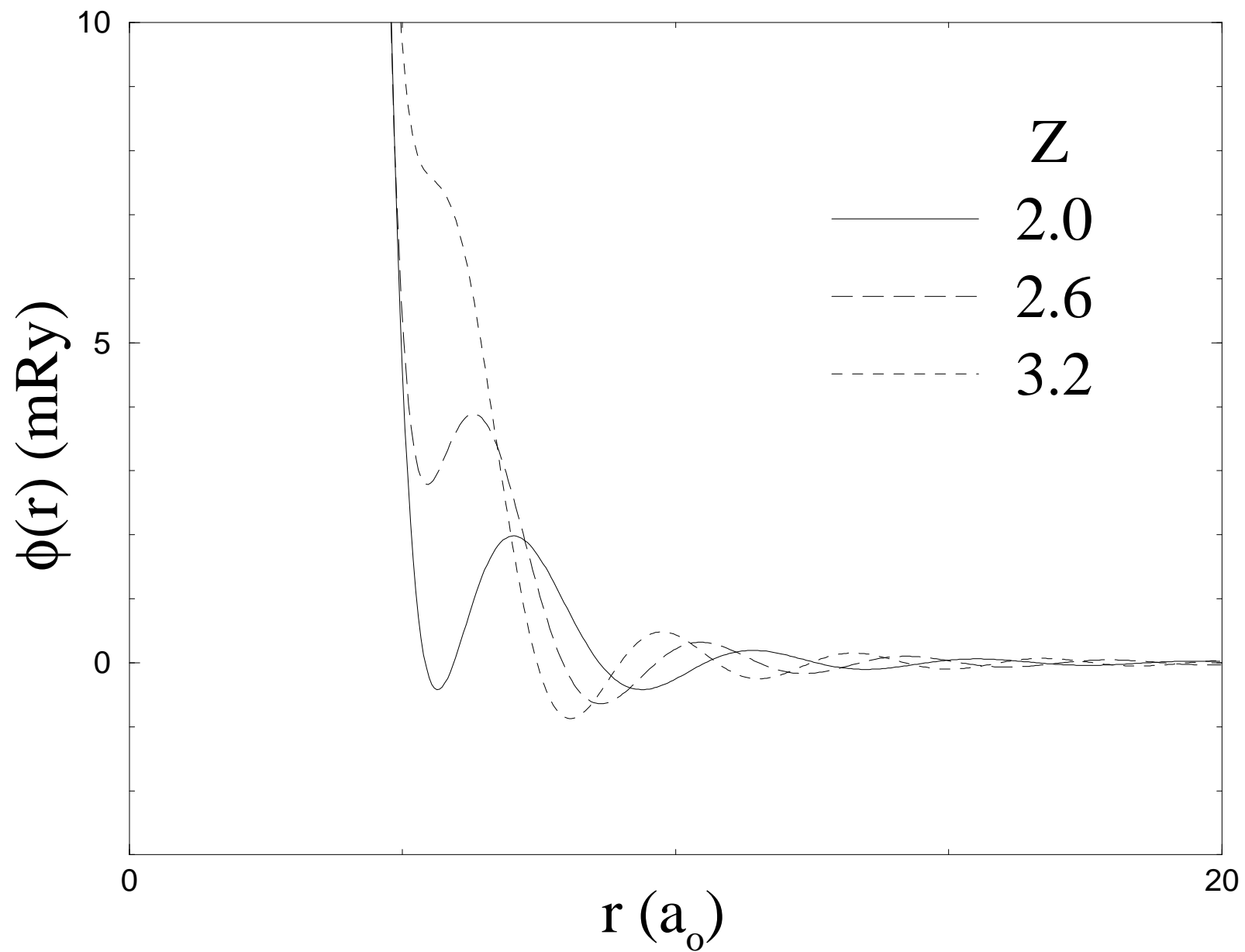


Fig. 1b (Denton and Hafner)

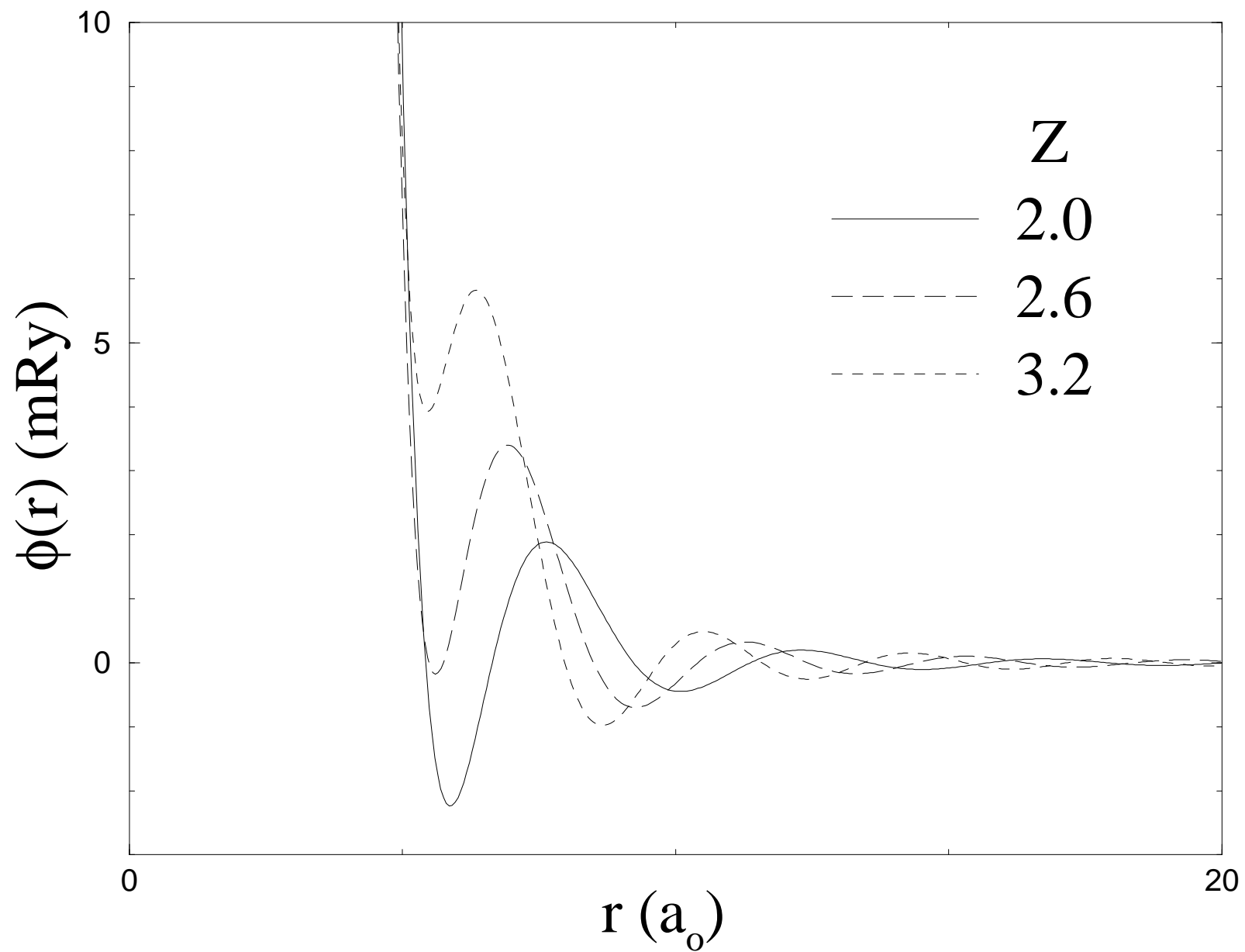


Fig. 1c (Denton and Hafner)

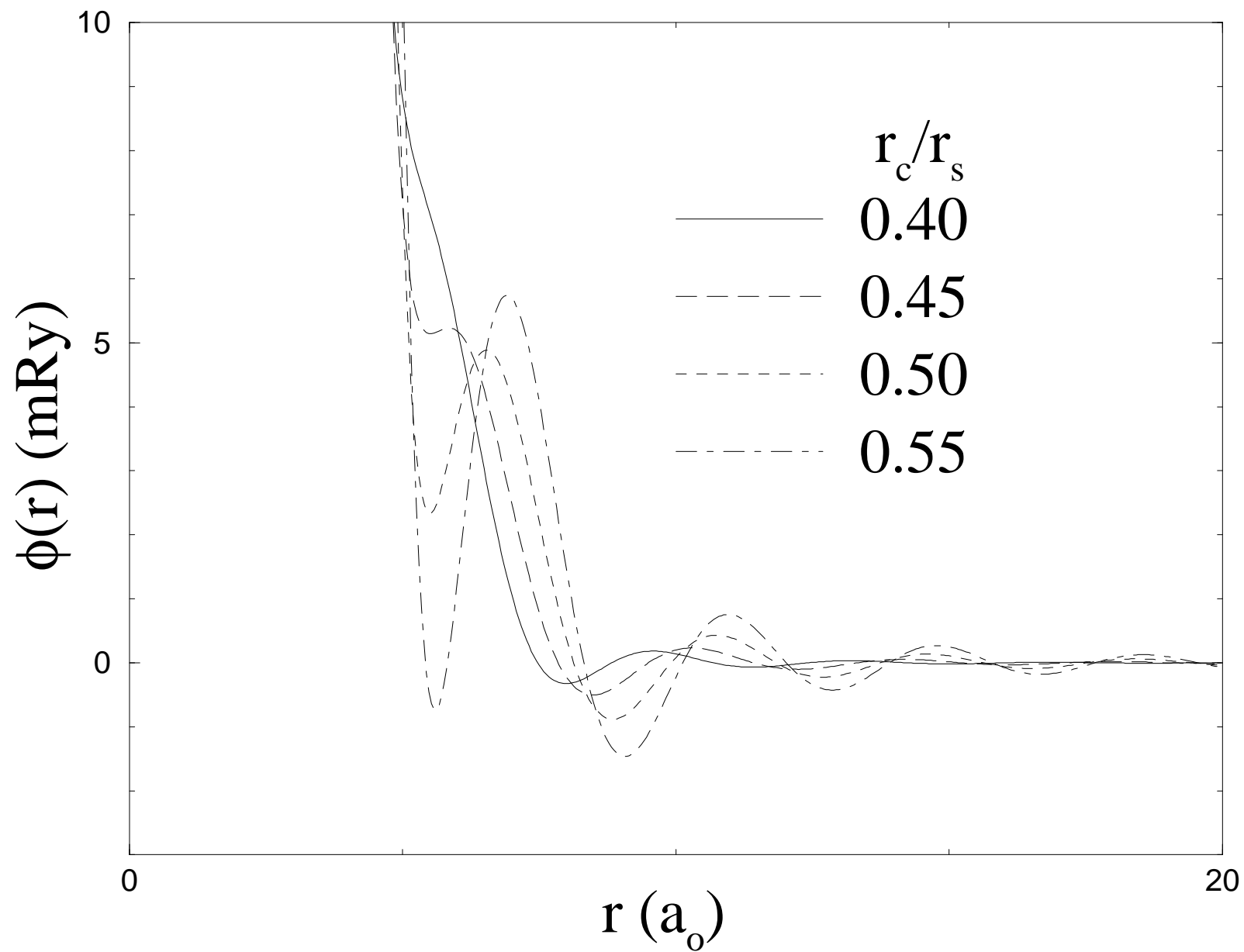


Fig. 2 (Denton and Hafner)

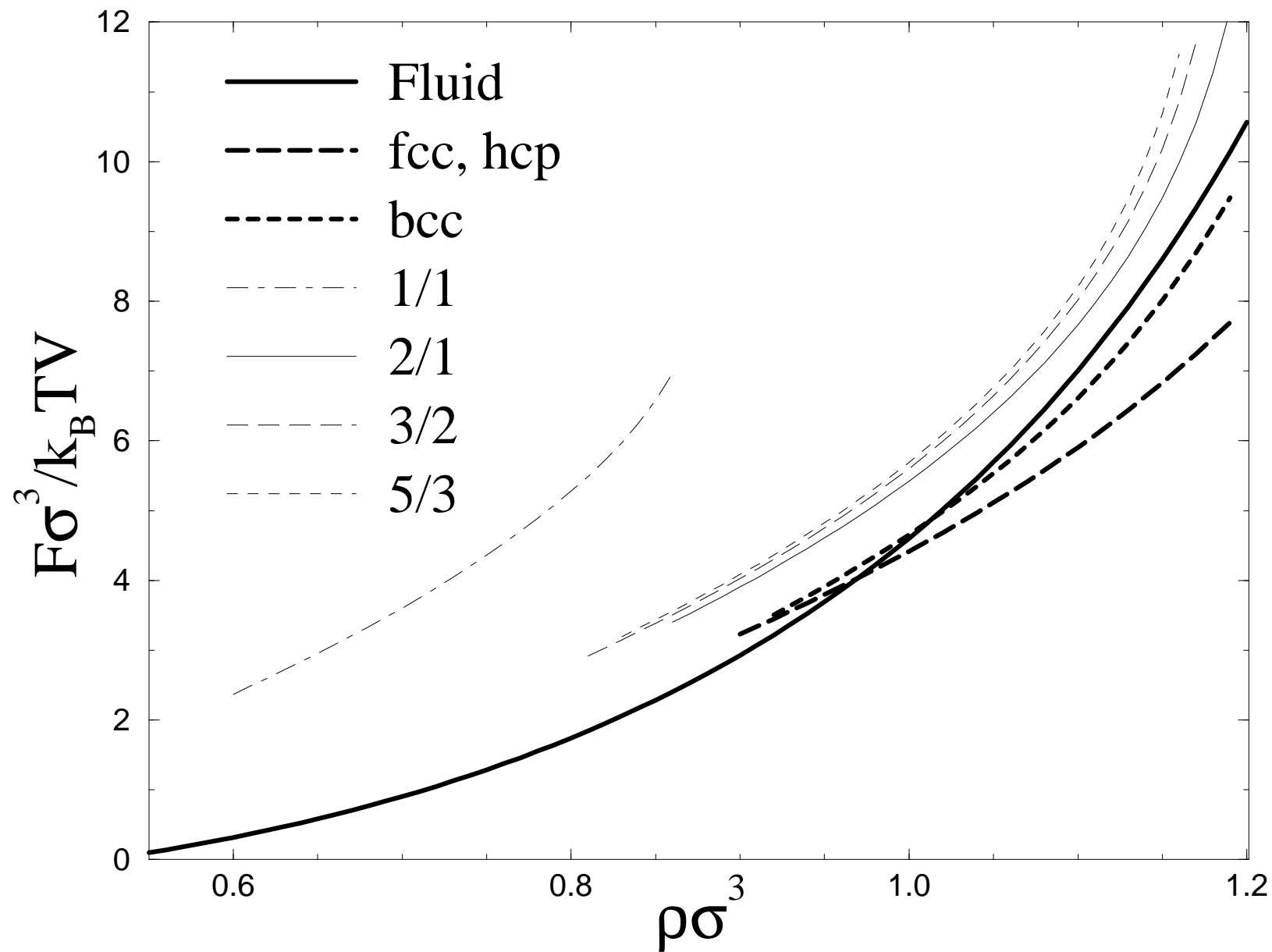


Fig. 3a (Denton and Hafner)

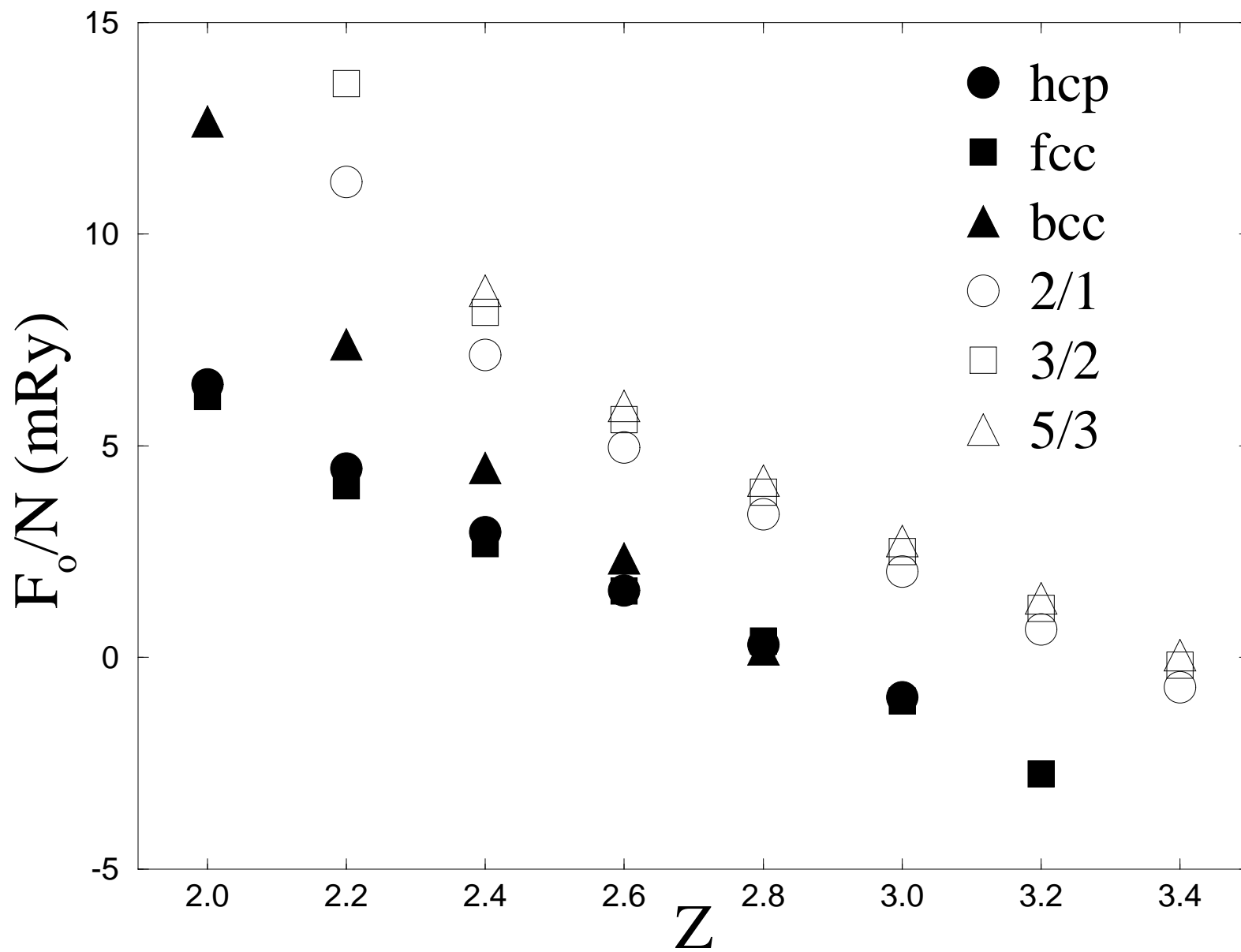


Fig. 3b (Denton and Hafner)

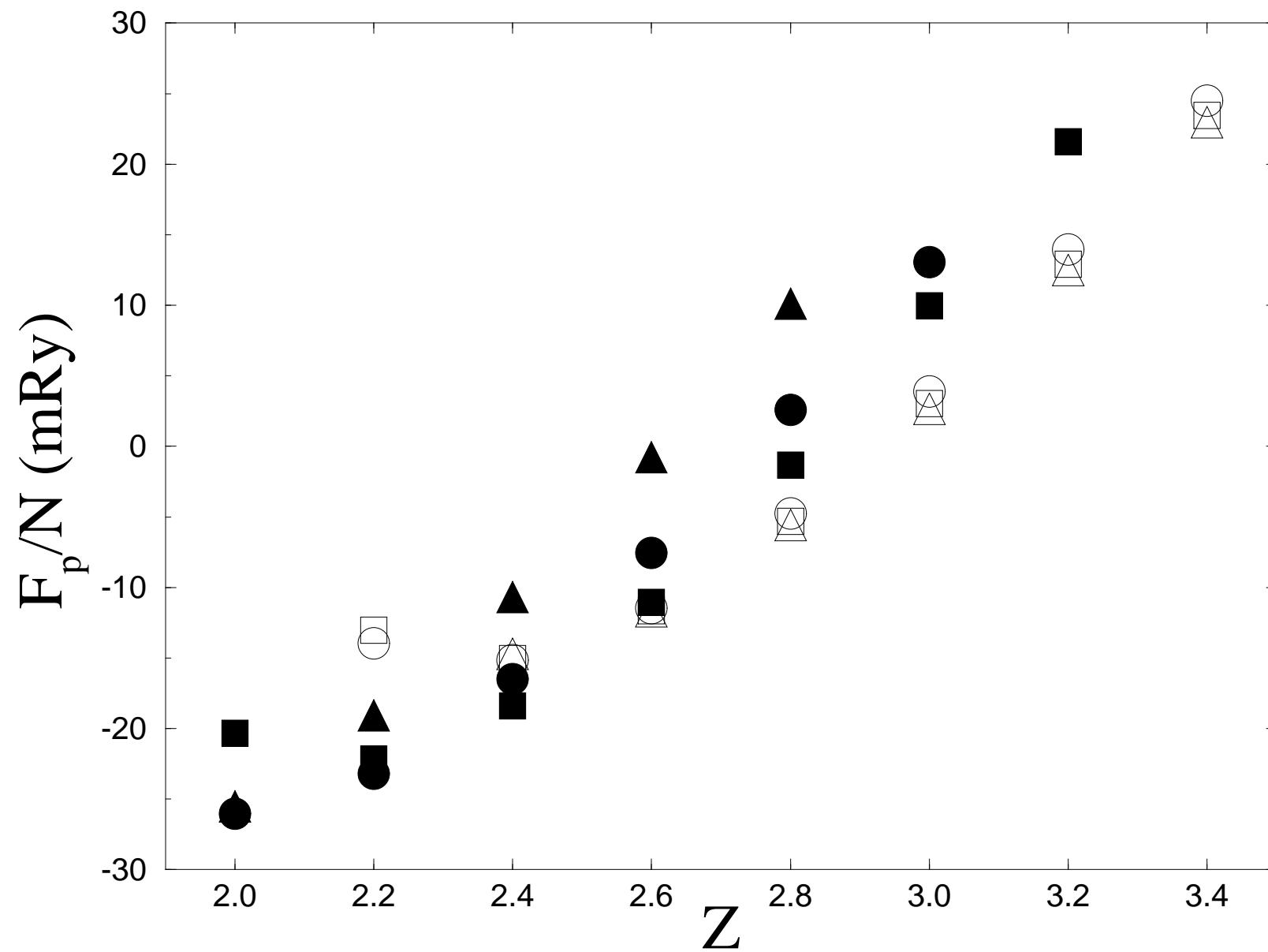


Fig. 4 (Denton and Hafner)

